Demonstration of Tunable Three-Body Interactions between Superconducting Qubits

Tim Menke,[1,2,3,*,‡] William P. Banner,[4,‡] Thomas R. Bergamaschi,[1] Agustin Di Paolo,[1] Antti Vepsäläinen,[1] Steven J. Weber,[5] Roni Winik,[1] Alexander Melville,[5] Bethany M. Niedzielski,[5] Danna Rosenberg,[5] Kyle Serniak,[5] Mollie E. Schwartz,[5] Jonilyn L. Yoder,[5] Alán Aspuru-Guzik,[6,7,8] Simon Gustavsson,[1] Jeffrey A. Grover,[1] Cyrus F. Hirjibehedin,[5] Andrew J. Kerman,[5] and William D. Oliver[1,2,4,5,†]

[1]*Research Laboratory of Electronics, Massachusetts Institute of Technology, Cambridge, Massachusetts 02139, USA*
[2]*Department of Physics, Massachusetts Institute of Technology, Cambridge, Massachusetts 02139, USA*
[3]*Department of Physics, Harvard University, Cambridge, Massachusetts 02138, USA*
[4]*Department of Electrical Engineering and Computer Science, Massachusetts Institute of Technology, Cambridge, Massachusetts 02139, USA*
[5]*Lincoln Laboratory, Massachusetts Institute of Technology, Lexington, Massachusetts 02421-6426, USA*
[6]*Departments of Chemistry and Computer Science, University of Toronto, Toronto, Ontario M5G 1Z8, Canada*
[7]*Vector Institute for Artificial Intelligence, Toronto, Ontario M5S 1M1, Canada*
[8]*Canadian Institute for Advanced Research, Toronto, Ontario M5G 1Z8, Canada*

(Received 17 April 2022; accepted 17 October 2022; published 21 November 2022)

Nonpairwise multiqubit interactions present a useful resource for quantum information processors. Their implementation would facilitate more efficient quantum simulations of molecules and combinatorial optimization problems, and they could simplify error suppression and error correction schemes. Here, we present a superconducting circuit architecture in which a coupling module mediates two-local and three-local interactions between three flux qubits by design. The system Hamiltonian is estimated via multiqubit pulse sequences that implement Ramsey-type interferometry between all neighboring excitation manifolds in the system. The three-local interaction is coherently tunable over several MHz via the coupler flux biases and can be turned off, which is important for applications in quantum annealing, analog quantum simulation, and gate-model quantum computation.

DOI: 10.1103/PhysRevLett.129.220501

A key challenge in the development of quantum computers is the implementation of resource-efficient and precisely tunable interactions between qubits [1]. To date, most of the interactions that have been implemented in quantum systems are pairwise in nature. While pairwise interactions, which are referred to as two-local, are sufficient to generate entanglement across a many-qubit system [2–4], there are many cases, particularly when using limited-depth circuits, in which such interactions are insufficient or inconvenient: multiqubit interactions are a prerequisite for analog quantum simulations of chemistry Hamiltonians and certain condensed matter physics models [5,6] as well as for quantum annealing for combinatorial optimization [7–9]. They play a key role in error suppression schemes [10] and in parity checks for error correction algorithms [11].

Experimental demonstrations of multiqubit interactions are scarce: a four-local ring exchange has been observed in a cold-atom system when suppressing lower-order interactions [12], and a small, chiral three-local interaction has been engineered between dynamically driven superconducting qubits [13]. Thus far, the interactions have been slow and not suitable for use in a scalable quantum information processing architecture. In addition, few metrological methods exist to extract all interactions of a nonpairwise coupled system precisely [14]. However, significant interest in multiqubit coupling mechanisms persists, as evidenced by a number of proposals for tunable multiqubit couplers for quantum processors [15–21].

In this Letter, we demonstrate tunable three-local interactions between superconducting flux qubits. The interactions are mediated by a coupler circuit, which enables static coupling without the need for dynamic driving. This eliminates the potential for unwanted leakage out of the computational subspace as well as the generation of spurious sidebands, which can occur during high-power driving [22]. A multiqubit Hamiltonian estimation technique is implemented to determine the system parameters: the coherence of the qubits, which is drastically improved over typical annealing-type qubits, is exploited to implement multiqubit Ramsey sequences for precise metrology of the system eigenenergies. This technique distinguishes the three-local coupling from each individual two-local interaction between the qubits. We find that the three-local coupling strength can be tuned from an essentially off bias point to a maximal strength of -6.5 MHz, which is comparable to typical interaction rates in certain state-of-the-art digital processors [23] and could enable gate times of a few hundred

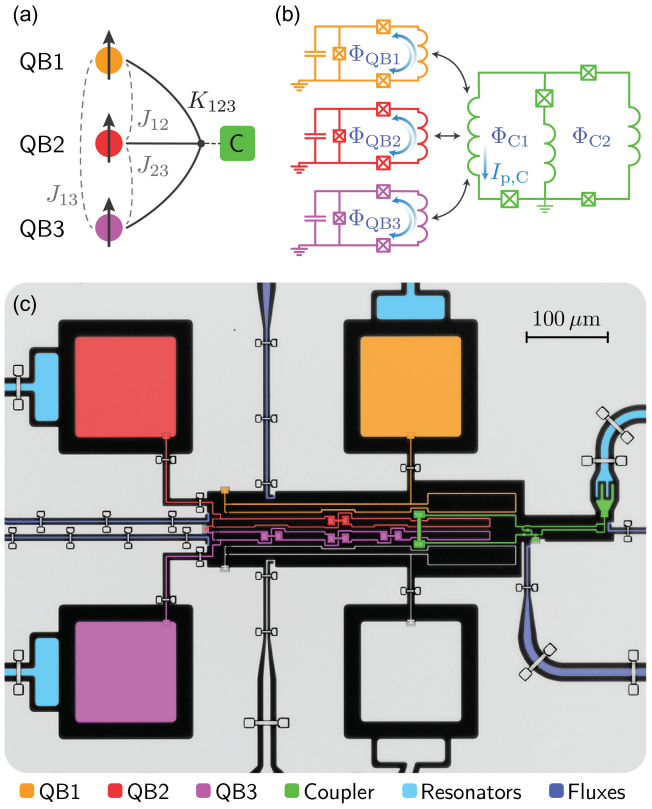

FIG. 1. Coupled multiqubit system. (a) The qubits are coupled to a common coupler C, which mediates a 3-qubit interaction. Spurious terms of lower locality are included in the model (dashed lines). (b) Superconducting circuit that implements the desired system. It is constructed from flux qubits that couple inductively and capacitively to the coupler circuit. External fluxes Φ determine the local spin fields and coupler properties. (c) Micrograph of the on-chip realization of the circuit.

nanoseconds. Numerical simulations of the full circuit Hamiltonian elucidate the coupling mechanism and show that it arises from interactions between the coupler excited state and higher excited states of the qubit system. The coupling is also tunable by about 3 MHz along a flux insensitive path in the coupler dispersion, preserving maximum qubit coherence. Therefore, our Letter presents both a demonstration of an elusive coupling mechanism and a solution for more resourceful interactions in quantum processors.

We consider a system of three qubits that are pairwise coupled both among themselves and to a coupler element [see Fig. 1(a)]. The qubits are modeled as spins that are aligned or antialigned with the z axis, with the ground (excited) state given by $|0\rangle$ ($|1\rangle$). The coupler element induces a nonpairwise three-local interaction as well as spurious two-local interactions, which add to the existing capacitive and inductive two-local interactions. As the coupler has a larger frequency gap than the qubits and is not excited during operations, we can model the system as an effective 3-qubit system with the following eigenbasis Hamiltonian:

$$H/\hbar = -\sum_{i=1}^{3}\frac{\omega_i}{2}\hat{Z}_i + \sum_{\substack{i,j=1\\ i<j}}^{3} J_{ij}\hat{Z}_i\hat{Z}_j + K_{123}\hat{Z}_1\hat{Z}_2\hat{Z}_3, \quad (1)$$

where ω_i denotes the single-qubit frequencies, J_{ij} the two-local, and K_{123} the three-local coupling strengths. The Pauli $\hat{Z}$ matrix for qubit i is given by $\hat{Z}_i$.

The system is implemented as a superconducting circuit that consists of three flux qubits [24–26] and a flux tunable coupler [21,27] [see Fig. 1(b)]. The flux qubit eigenstates are superpositions of clockwise and counterclockwise circulating currents in the qubit loop. Throughout this Letter, the qubits are operated at the flux insensitive point, which occurs when the external flux threading the loop is $\Phi_{QBi} = 0.5\ \Phi_0$. At this flux bias, the three qubit frequencies Δ_{QBi} are in the range of 2.5–5.5 GHz. Before diagonalizing the system to obtain the form of Eq. (1), each flux qubit is described by the following Hamiltonian in the persistent-current basis:

$$H_{QBi}/\hbar = \varepsilon(\Phi_{QBi})\hat{z}_i + \Delta_{QBi}\hat{x}_i, \quad (2)$$

where $\hat{z}_i$ and $\hat{x}_i$ are the Pauli matrices specified in the persistent-current basis and the flux insensitive point is parametrized to $\varepsilon = 0$. The pairwise coupling to other qubits and the coupler includes both inductive and capacitive interactions.

The coupler circuit was first proposed in Refs. [21,28] and shown experimentally to exhibit a nonlinear coupling potential versus flux [27]. It is therefore expected to mediate nonpairwise interactions when inductively coupled to a set of flux qubits. At the same time, the excited state of the coupler can push down the qubit energy levels and induce effective interactions in the qubit subspace when biased around its minimum frequency gap of about 9 GHz. In order to predict the system couplings, we numerically simulate the circuit Hamiltonian in a mixed representation of the charge and harmonic oscillator bases, using a hierarchical diagonalization strategy to solve the qubit and coupler Hamiltonians separately before adding the interactions [29].

The circuit was fabricated with a high-quality aluminum-based process patterned on a silicon substrate, embedded in readout and control infrastructure as shown in Fig. 1(c) [26]. The qubit loops are elongated to encompass surface area within or in proximity to the left coupler loop, thereby coupling the qubits inductively and capacitively to the coupler. In two of the qubit loops, bowtie-shaped crossovers are used to route wires over one another and connect ground planes and twist the loops [30]. These twists reduce the inductive coupling between the qubits. Individual readout resonators are capacitively coupled to the shunt capacitor of each qubit, with a state-dependent resonator shift χ_i between 2–20 MHz at the flux insensitive point and coupling rate $\kappa_i/2\pi = 1$–2 MHz to a shared feedline, which

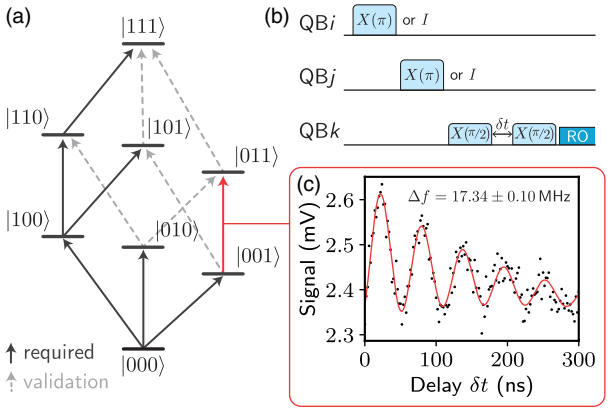

FIG. 2. Hamiltonian estimation method. (a) Energy level diagram of the 3-qubit system. The allowed single-photon transitions are indicated with arrows. The 3-qubit Hamiltonian model is fully determined by a subset of transitions (solid black). The other transitions are used to validate the model. (b) Multiqubit pulse sequence that implements Ramsey interferometry between arbitrary single-photon transitions. (c) Example Ramsey interferometry data for the $|001\rangle \rightarrow |011\rangle$ transition. The fit is used to determine the transition frequency precisely, which is determined by the sum of the drive frequency and the extracted detuning Δf.

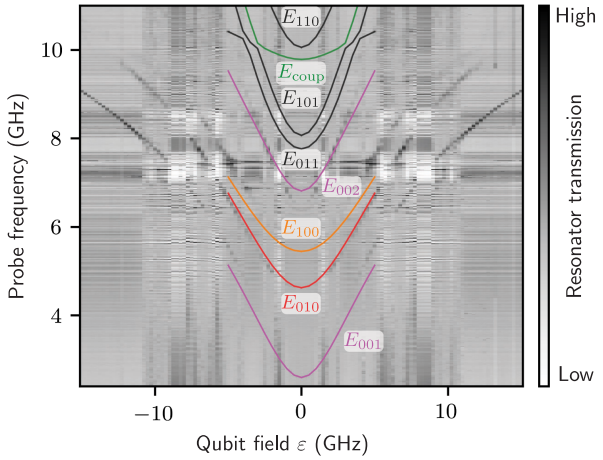

FIG. 3. Spectroscopy of the system at maximum coupling around the flux insensitive point $\varepsilon = 0$ of the qubits. The excited states of the qubits as well as some higher-lying states are visible. Eigenenergies obtained from a full circuit Hamiltonian model are overlaid. The data are acquired by strongly driving the circuit through a shared feedline and reading out the QB3 resonator. The vertical and horizontal lines are artifacts stemming from qubit-resonator hybridization and interference of the spectroscopy tones, respectively.

enables fast readout with a 360 ns integration time. Qubit operations are implemented by resonantly driving the qubit through the resonator. Local flux lines permit control of the individual loop fluxes. Flux crosstalk to nonprimary loops is suppressed to a mean of 0.5% and maximum of 3.4% between any antenna-loop pair via an iterative calibration procedure based on Refs. [27,31]. For details on the procedure, we refer to the Supplemental Material [34]. The on-chip circuit includes a fourth flux qubit that is not needed and so was far detuned from the other transitions.

In order to estimate the Hamiltonian of the 3-qubit system and extract its interactions, we measure the eigenenergies of the system up to a total of three excitations, one per qubit. The transitions between eigenstates in adjacent excitation manifolds are shown in Fig. 2(a). Each transition frequency is a linear combination of the Hamiltonian parameters in the eigenbasis of the full system. If we are able to identify and precisely measure a set of transitions that include each eigenstate at least once, the Hamiltonian parameters in Eq. (1) can be determined by inverting a linear system of equations. We use a Ramsey interferometry experiment to determine each transition frequency [32]—for example, for the transition $|001\rangle \rightarrow |011\rangle$ [see Figs. 2(b) and 2(c)]. It is realized by applying successive π pulses such that the system is driven from the ground state to the lower state of the transition of interest, which in the example case requires the sequence

$$|000\rangle \xrightarrow{X_3(\pi)} |001\rangle. \tag{3}$$

The Ramsey experiment then proceeds with 20-ns long $\pi/2$ pulses slightly detuned from the desired transition, separated by a time delay δt and followed by a readout pulse. The precise transition frequency is manifest in the Ramsey fringe oscillation frequency, which is determined from a fit to the data of a sinusoid that includes the T_1 decay of the other qubits [see Fig. 2(c)]. The error is estimated as the one-sigma confidence interval for the fit parameter [33].

It is essential for the Hamiltonian estimation method that the computational eigenstates are correctly identified, which is generally a challenge for strongly coupled systems. We first perform qubit spectroscopy to determine the lowest three transitions in the system, which correspond to single-qubit excitations. In Fig. 3, we show a qubit spectroscopy dataset that is obtained by sweeping the frequency of a continuous-wave tone and monitoring the resonator coupled to QB3. In this measurement, coupling between each qubit and the three resonators was used as a resource, as it makes visible the excited states of all three qubits as well as some higher excited states in a single two-dimensional scan. Having identified the lowest transitions, we proceed to find successively higher transitions in the computational subspace by applying π pulses to lower transitions and performing Rabi spectroscopy around the bare frequency of the respective qubit. To exclude the mislabeling of undesired multiphoton transitions, we double the drive amplitude and check that the Rabi oscillation frequency also doubles. In addition, after all transitions are identified and measured via the multiqubit Ramsey protocol, we use a minimal subset of transitions to predict the remaining ones. By finding that the predictions match the measurements to within the error estimates, we have verified that the identified transitions connect a closed set of

computational states. We refer the reader to the Supplemental Material [34] for additional details about the eigenstate verification procedure. The set of computational states is then used to fit a full circuit Hamiltonian model to the spectroscopy data, which is overlaid with that data in Fig. 3 for all states, including those that do not appear in the spectroscopy. The model is valid around the flux insensitive point of the qubits, which corresponds to $\varepsilon = 0$. In addition, it approximately captures the second excited state energy E_{002} of QB3 as well as the coupler excited state energy E_{coup}, which are faintly visible in the spectrum.

The interactions between the qubits can be tuned by changing the flux bias point of the coupler circuit. The flux tuning landscape of the coupler is shown in Fig. 4(a). The dark, diagonal feature in the transmission spectrum indicates the flux manifold along which the coupler frequency gap is minimal [27]. It arises from the coupler excited state pushing the coupler resonator down in frequency via dispersive interaction. Simulations of the circuit predict maximum three-local coupling in this regime.

We identify two distinct tuning paths for the three-local coupling between the qubits. The first is a vertical "on-off" path along Φ_{C2} with fixed Φ_{C1}, which enables the maximum range of K_{123} including zero coupling. The three-local coupling is tuned from 0.8 to −4.6 MHz along this path, as seen in the visualization of the extracted couplings in Fig. 4(b). These Hamiltonian parameters are extracted using the estimation procedure that was described above at each flux point. We also observe that the local qubit fields and two-local interactions between the qubits are modified by the coupler. When using the coupler for practical applications, additional two-local couplers for each qubit pair can be used to eliminate such spurious couplings and tune all Hamiltonian parameters independently [37]. The qubit decoherence rates are largest in the steepest region of the coupler spectrum. Higher coherence is recovered at the point of maximum two-local coupling, which is a flux insensitive point of the coupler.

The interactions in the 3-qubit system are a combination of two contributions: first, the computational states of the isolated qubit circuits interact directly, which leads to two-local interactions in the effective spin model. Second, capacitive and inductive interactions between the computational and higher excited modes of the circuit modify both the two-local and three-local interactions. As a result, a small three-local coupling of 0.51 MHz is present even when the coupler is turned off and the coupler excited state is far detuned ($\Phi_{C2} = 0\ \Phi_0$). When the coupler is turned on ($\Phi_{C2} \sim 0.5\ \Phi_0$), its frequency gap drops to about 9.5 GHz and the coupler excited state interacts with nearby qubit modes. Numerical simulations of the full circuit Hamiltonian reveal an approximate picture of the higher-excited state frequencies, which is detailed in the Supplemental Material [34]. Repulsion or attraction between the coupler excited state and the qubit modes, most prominently the computational states $|101\rangle$ and $|110\rangle$, modifies the effective spin Hamiltonian of the system. As a result, the coupling strengths in the effective spin system are modified. The tuning rate is highest when the coupler flux is close to 0.5 Φ_0, which is when the coupler dispersion is steepest and its frequency is lowest. The measured coupling parameters in Fig. 4(b) reflect this tuning behavior, which validates our understanding of the multimode system.

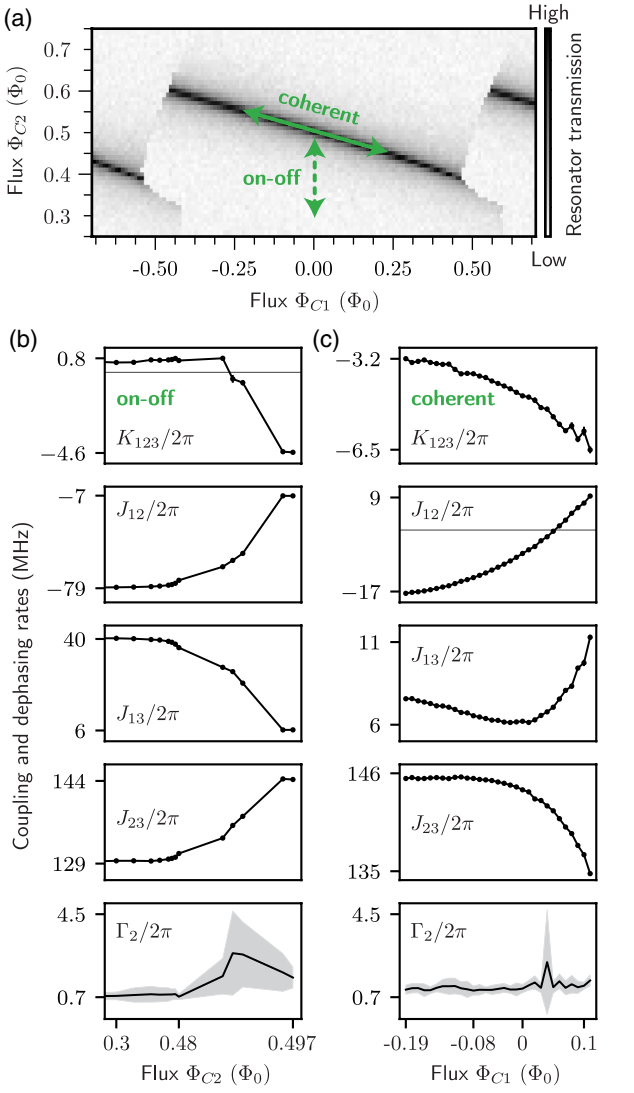

FIG. 4. Tuning of the qubit interactions with coupler flux bias. (a) Transmission spectrum of the coupler resonator versus the coupler fluxes. Transmission is measured at a fixed frequency below the bare resonator frequency. (b) Tunability of the interactions is largest along the on-off direction. Shown are the three-local interaction K_{123}, the two-local interactions J_{ij}, and the mean decoherence rates Γ_2. Error bars for the couplings are smaller than the markers unless visible, and the shaded area for Γ_2 indicates the standard deviation between the decoherence rates of all transitions. (c) The couplings can also be varied along the noise insensitive diagonal feature of the coupler spectrum, which is optimal for quantum simulation.

The second tuning path follows the diagonal feature, and it enables tunability of K_{123} between -3.2 and -6.5 MHz. It preserves maximum coherence of the qubits as the coupler stays first-order insensitive to flux noise at these fluxes. The stable coherence is evident in the bottom panel of Fig. 4(c). In addition, all the interactions tune smoothly, and the change in spurious two-local coupling is smaller than in the on-off tuning direction. As a result, the coherent tuning regime is suitable for variations of the coupling during analog simulations or for digital gates, whereas the on-off tuning path is optimal for quickly turning the coupling on or off during an annealing protocol.

In conclusion, we have demonstrated a coherent quantum system that exhibits tunable multibody interactions. Multiqubit effects are of fundamental interest as they do not arise naturally in nonrelativistic quantum systems, and they provide a resource for analog quantum simulation, problem Hamiltonian engineering for quantum annealing, and gate design for digital algorithms. In our demonstration, the system Hamiltonian is estimated via digital multiqubit pulse sequences that precisely determine the frequencies of all computational eigenstates, enabling the distinct identification of three-local interactions in the presence of lower-order couplings. We study two different tuning regimes for the three-local coupling and identify interactions between higher-excited states of the circuit as the source of the effective interaction. The coherence times of the qubits, which we expect to be limited by flux noise from on-chip sources [38], can be improved by reducing the loop size of the flux qubits and coupler as well as by 3D integration [30]. The required coupling can then be boosted by connecting the circuit elements galvanically rather than by a mutual inductance. This should greatly improve lifetimes across the circuit as the coupling mechanism itself does not seem to intrinsically limit qubit lifetimes, as shown in the Supplemental Material [34]. We highlight that the coupling scheme is compatible with other qubit modalities such as the transmon [39] or fluxonium qubit [40] and thus could serve as an efficient resource for gate-model quantum applications. In particular, either the longer coherence of these qubits or a larger interaction strength stemming from galvanic coupling could enable 3-qubit gates that are faster than the coherence time. We also note that the coherence times demonstrated here are already sufficient for quantum annealing applications and merely require the use of stronger multiqubit interactions. Methods of strengthening this coupling even further have been investigated previously and could be implemented in future work [20]. The studied superconducting circuit includes an additional flux qubit, which can be used to demonstrate 4-body interactions. Moreover, the coupling scheme is extensible to even higher orders of interactions by adding additional loops to the coupler circuit [27].

It is a pleasure to thank X. Dai and F. Wilhelm-Mauch for valuable discussions, D. K. Kim for assistance with the fabrication, and J. I-J. Wang for taking the optical micrograph of the device. This research was funded in part by the Office of the Director of National Intelligence (ODNI), Intelligence Advanced Research Projects Activity (IARPA) under Air Force Contract No. FA8702-15-D-0001. The views and conclusions contained herein are those of the authors and should not be interpreted as necessarily representing the official policies or endorsements, either expressed or implied, of the ODNI, IARPA, or the U.S. Government.

*Corresponding author.
timmenke@mit.edu
†Corresponding author.
william.oliver@mit.edu
‡These authors contributed equally to the work

[1] M. Kjaergaard, M. E. Schwartz, J. Braumüller, P. Krantz, J. I.-J. Wang, S. Gustavsson, and W. D. Oliver, Superconducting qubits: Current state of play, Annu. Rev. Condens. Matter Phys. **11**, 369 (2020).
[2] R. Barends, J. Kelly, A. Megrant, A. Veitia, D. Sank, E. Jeffrey, T. C. White, J. Mutus, A. G. Fowler, B. Campbell *et al.*, Superconducting quantum circuits at the surface code threshold for fault tolerance, Nature (London) **508**, 500 (2014).
[3] H. Bernien, S. Schwartz, A. Keesling, H. Levine, A. Omran, H. Pichler, S. Choi, A. S. Zibrov, M. Endres, M. Greiner *et al.*, Probing many-body dynamics on a 51-atom quantum simulator, Nature (London) **551**, 579 (2017).
[4] K. A. Landsman, C. Figgatt, T. Schuster, N. M. Linke, B. Yoshida, N. Y. Yao, and C. Monroe, Verified quantum information scrambling, Nature (London) **567**, 61 (2019).
[5] R. Babbush, P. J. Love, and A. Aspuru-Guzik, Adiabatic quantum simulation of quantum chemistry, Sci. Rep. **4**, 1 (2014).
[6] K. Majumdar, D. Furton, and G. S. Uhrig, Effects of ring exchange interaction on the Néel phase of two-dimensional, spatially anisotropic, frustrated Heisenberg quantum antiferromagnet, Phys. Rev. B **85**, 144420 (2012).
[7] R. Martoňák, G. E. Santoro, and E. Tosatti, Quantum annealing of the Traveling-Salesman problem, Phys. Rev. E **70**, 057701 (2004).
[8] G. E. Santoro and E. Tosatti, Optimization using quantum mechanics: Quantum annealing through adiabatic evolution, J. Phys. A **39**, R393 (2006).
[9] P. Hauke, H. G. Katzgraber, W. Lechner, H. Nishimori, and W. D. Oliver, Perspectives of quantum annealing: Methods and implementations, Rep. Prog. Phys. **83**, 054401 (2020).
[10] D. Bacon, Operator quantum error-correcting subsystems for self-correcting quantum memories, Phys. Rev. A **73**, 012340 (2006).
[11] A. G. Fowler, M. Mariantoni, J. M. Martinis, and A. N. Cleland, Surface codes: Towards practical large-scale quantum computation, Phys. Rev. A **86**, 032324 (2012).
[12] H.-N. Dai, B. Yang, A. Reingruber, H. Sun, X.-F. Xu, Y.-A. Chen, Z.-S. Yuan, and J.-W. Pan, Four-body ring-exchange interactions and anyonic statistics within a minimal toric-code hamiltonian, Nat. Phys. **13**, 1195 (2017).

[13] W. Liu, W. Feng, W. Ren, D.-W. Wang, and H. Wang, Synthesizing three-body interaction of spin chirality with superconducting qubits, Appl. Phys. Lett. **116**, 114001 (2020).
[14] T. R. Bergamaschi, T. Menke, W. P. Banner, A. Di Paolo, S. J. Weber, C. F. Hirjibehedin, A. J. Kerman, and W. D. Oliver, Distinguishing multi-spin interactions from lower-order effects, arXiv:2111.12717.
[15] A. Mezzacapo, L. Lamata, S. Filipp, and E. Solano, Many-Body Interactions with Tunable-Coupling Transmon Qubits, Phys. Rev. Lett. **113**, 050501 (2014).
[16] M. Hafezi, P. Adhikari, and J. M. Taylor, Engineering three-body interaction and Pfaffian states in circuit QED systems, Phys. Rev. B **90**, 060503(R) (2014).
[17] N. Chancellor, S. Zohren, and P. A. Warburton, Circuit design for multi-body interactions in superconducting quantum annealing systems with applications to a scalable architecture, npj Quantum Inf. **3**, 21 (2017).
[18] D. Kafri, C. Quintana, Y. Chen, A. Shabani, J. M. Martinis, and H. Neven, Tunable inductive coupling of superconducting qubits in the strongly nonlinear regime, Phys. Rev. A **95**, 052333 (2017).
[19] M. Schöndorf and F. K. Wilhelm, Nonpairwise Interactions Induced by Virtual Transitions in Four Coupled Artificial Atoms, Phys. Rev. Appl. **12**, 064026 (2019).
[20] D. Melanson, A. J. Martinez, S. Bedkihal, and A. Lupascu, Tunable three-body coupler for superconducting flux qubits, arXiv:1909.02091.
[21] T. Menke, F. Häse, S. Gustavsson, A. J. Kerman, W. D. Oliver, and A. Aspuru-Guzik, Automated discovery of superconducting circuits and its application to 4-local coupler design, arXiv:1912.03322.
[22] M. Reagor *et al.*, Demonstration of universal parametric entangling gates on a multi-qubit lattice, Sci. Adv. **4**, eaao3603 (2018).
[23] Y. Sung, L. Ding, J. Braumüller, A. Vepsäläinen, B. Kannan, M. Kjaergaard, A. Greene, G. O. Samach, C. McNally, D. Kim *et al.*, Realization of High-Fidelity CZ and ZZ-Free iSWAP Gates with a Tunable Coupler, Phys. Rev. X **11**, 021058 (2021).
[24] T. P. Orlando, J. E. Mooij, L. Tian, C. H. Van Der Wal, L. Levitov, S. Lloyd, and J. J. Mazo, Superconducting persistent-current qubit, Phys. Rev. B **60**, 15398 (1999).
[25] J. Q. You, X. Hu, S. Ashhab, and F. Nori, Low-decoherence flux qubit, Phys. Rev. B **75**, 140515(R) (2007).
[26] F. Yan, S. Gustavsson, A. Kamal, J. Birenbaum, A. P. Sears, D. Hover, T. J. Gudmundsen, D. Rosenberg, G. Samach, S. Weber *et al.*, The flux qubit revisited to enhance coherence and reproducibility, Nat. Commun. **7**, 1 (2016).
[27] T. Menke, Classical and quantum optimization of quantum processors, Doctoral dissertation, Harvard University (2022).
[28] A. Kerman, Design and simulation of complex superconducting circuits for advanced quantum annealing hardware, Am. Phys. Soc. **2018**, C26 (2018).
[29] A. J. Kerman, Efficient numerical simulation of complex Josephson quantum circuits, arXiv:2010.14929.
[30] D. Rosenberg, S. J. Weber, D. Conway, D.-R. W. Yost, J. Mallek, G. Calusine, R. Das, D. Kim, M. E. Schwartz, W. Woods *et al.*, Solid-state qubits: 3d integration and packaging, IEEE Microw. Mag. **21**, 72 (2020).
[31] X. Dai, D. M. Tennant, R. Trappen, A. J. Martinez, D. Melanson, M. A. Yurtalan, Y. Tang, S. Novikov, J. A. Grover, S. M. Disseler, J. I. Basham, R. Das, D. K. Kim, A. J. Melville, B. M. Niedzielski, S. J. Weber, J. L. Yoder, D. A. Lidar, and A. Lupascu, Calibration of flux crosstalk in large-scale flux-tunable superconducting quantum circuits, PRX Quantum **2**, 040313 (2021).
[32] N. F. Ramsey, A molecular beam resonance method with separated oscillating fields, Phys. Rev. **78**, 695 (1950).
[33] M. Newville, T. Stensitzki, D. B. Allen, M. Rawlik, A. Ingargiola, and A. Nelson, LMFIT: Non-linear least-square minimization and curve-fitting for python, Astrophysics Source Code Library, ascl (2016).
[34] See Supplemental Material, which includes Refs. [35,36], at http://link.aps.org/supplemental/10.1103/PhysRevLett.129.220501 for additional information on the experimental setup, system properties, calibration procedures, measurement and simulation techniques, as well as Supplemental Figs. 1–8.
[35] O. Yaakobi, L. Friedland, C. Macklin, and I. Siddiqi, Parametric amplification in Josephson junction embedded transmission lines, Phys. Rev. B **87**, 144301 (2013).
[36] C. Macklin, K. O'Brien, D. Hover, M. E. Schwartz, V. Bolkhovsky, X. Zhang, W. D. Oliver, and I. Siddiqi, A near–quantum-limited Josephson traveling-wave parametric amplifier, Science **350**, 307 (2015).
[37] S. J. Weber, G. O. Samach, D. Hover, S. Gustavsson, D. K. Kim, A. Melville, D. Rosenberg, A. P. Sears, F. Yan, J. L. Yoder *et al.*, Coherent Coupled Qubits for Quantum Annealing, Phys. Rev. Appl. **8**, 014004 (2017).
[38] J. Braumüller, L. Ding, A. P. Vepsäläinen, Y. Sung, M. Kjaergaard, T. Menke, R. Winik, D. Kim, B. M. Niedzielski, A. Melville *et al.*, Characterizing and Optimizing Qubit Coherence Based on Squid Geometry, Phys. Rev. Appl. **13**, 054079 (2020).
[39] J. Koch, T. M. Yu, J. Gambetta, A. A. Houck, D. I. Schuster, J. Majer, A. Blais, M. H. Devoret, S. M. Girvin, and R. J. Schoelkopf, Charge-insensitive qubit design derived from the cooper pair box, Phys. Rev. A **76**, 042319 (2007).
[40] V. E. Manucharyan, J. Koch, L. I. Glazman, and M. H. Devoret, Fluxonium: Single cooper-pair circuit free of charge offsets, Science **326**, 113 (2009).